Synthesis and Characterization of Nickel Dithiocarbamate Complexes Bearing Ferrocenyl Subunits

Kenichi Oyaizu,[a] Kimihisa Yamamoto,[b] Yurie Ishii,[a] and Eishun Tsuchida*[a]

Abstract: Syntheses of a unique molecule, nickel(II) dithiocarbamate bearing two ferrocenyl groups (**3**), and its oxidized product, nickel(IV) dithiocarbamate bearing three ferrocenyl groups ($\mathbf{4}^+$), are reported. Spectroelectrochemical investigations have shown that the complex $\mathbf{4}^+$ undergoes a three-electron oxidation process, according to two quasireversible steps ($[Ni^{IV}(Fe^{II})_3]^+ \rightleftharpoons [Ni^{IV}(Fe^{II})_2Fe^{III}]^{2+}+e^-$, $[Ni^{IV}(Fe^{II})_2Fe^{III}]^{2+} \rightleftharpoons [Ni^{IV}(Fe^{III})_3]^{4+}+2e^-$), whose redox potentials are separated by $\Delta E = 250$ mV. The value ΔE is related to the comproportionation equilibrium ($[Ni^{IV}(Fe^{II})_3]^+ + [Ni^{IV}(Fe^{III})_2Fe^{II}]^{3+} \rightleftharpoons 2\,[Ni^{IV}Fe^{III}(Fe^{II})_2]^{2+}$) and results from the combination of a statistical contribution and a term which reflects the electrostatic repulsive interaction between the metal centers. In spite of the chemical equivalence of the three ferrocenyl groups, the mixed-valence state $[Ni^{IV}Fe^{III}(Fe^{II})_2]^{2+}$ ($\mathbf{4}^{2+}$) substantially persists in solution. Model studies with ethylene-bridged bis(ferrocenylimine) (**6**) have revealed that the electrostatic term is much lower in the absence of the nickel(IV) center. Preliminary force-field simulations on $\mathbf{4}^+$ have shown that enhanced electrostatic repulsion caused by the oxidation of the ferrocenyl subunits affects the conformation of the molecule, which results in a significant dimensional increment. Stereochemical features of the molecules are related to the electrostatic interaction and ΔG^0 associated with the comproportionation process is affected by such strong deformation that a decrease in electrostatic repulsion results.

Keywords: electrochemistry · metallocenes · N ligands · nickel · S ligands · sandwich complexes

Introduction

In an attempt to obtain molecular systems capable of exchanging more electrons with an electrode, the coupling of multiple, identical metal-centered fragments that individually display fast and reversible one-electron exchange has been performed.[1] A μ-oxo divanadium(IV) complex was previously shown by the authors to induce a two-electron transfer process.[2] In these systems, variation of the nature of the molecular framework that links the redox-active centers enable the extent of communication between the centers to be modulated, as reflected in the electrochemical response.[3] For instance, if electron communication between the two redox-active centers is *not* allowed and the distance between the two centers is large enough to minimize electrostatic repulsive interactions, the system will exchange two electrons through two one-electron processes whose potentials E_1 and E_2 are separated only by the statistical term $\Delta E = E_2 - E_1 = 35.6$ mV at 298 K.[4] On the other hand, intramolecular communication between the two metal centers causes the ΔE value to increase.[5] Such redox coupling has been discussed to occur through two main paths: (1) through-bond interactions, such as inductive effects, electron hopping, and electron delocalization through a bridging coordinating unit, and/or (2) through-space electrostatic and magnetic interactions. The extent of communication usually decreases as the distance between the metal centers is increased according to a hyperbolic mode. Indeed, molecular design of a framework that supports electronic interaction is an issue of recent interest as possible components of not only molecular electronic devices but also electron-storage systems.[6]

The redox behavior of linear triferrocenes in which ferrocenyl subunits are in close enough proximity to permit redox coupling has been described by a model in which initial oxidation occurs at both termini.[7] In contrast, reports on molecules that contain three or more ferrocenyl subunits in which the subunits are not linearly linked but appended to a central core are considerably less frequent.[8] We report here the synthesis and characterization of a nickel(IV) dithiocarbamate complex bearing three ferrocenyl subunits in which each ferrocenyl group is covalently linked to a central nickel(IV)

[a] Prof. Dr. E. Tsuchida, Dr. K. Oyaizu, Y. Ishii
Advanced Research Institute for Science and Engineering
Department of Polymer Chemistry
Waseda University
Tokyo 169-8555 (Japan)
Fax: (+81)3 3205-4740
E-mail: eishun@mn.waseda.ac.jp

[b] Prof. Dr. K. Yamamoto
Present address:
Department of Chemistry, Keio University, Yokohama 223 (Japan)

  0947-6539/99/0511-3193 $ 17.50+.50/0

core, and its very convenient electrosynthesis by use of a nickel(II) analogue bearing two ferrocenyl subunits. Electrochemical investigations revealed that, in spite of the chemical equivalence of the ferrocenyl groups, a mixed-valence state substantially persists in solution. An explanation for the stabilization of the mixed-valence state is provided in terms of the electrostatic effect.

Results and Discussion

Synthesis of the ligand 2 and Ni^{II} complexation: Our synthesis of the title complex hinged on the use of the new ligand **2**, which was prepared from ferrocenecarboxaldehyde by precedented Schiff-base formation and dithiocarbamation strategies (Scheme 1). Admixture of a 1:2 ratio of $NiCl_2$ and **2** in H_2O yielded analytically pure **3** in 90% yield as a green powder.

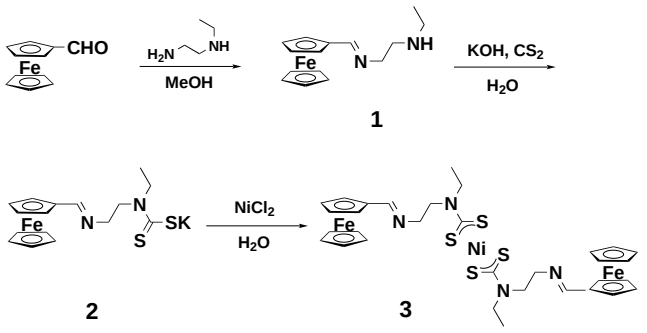

Scheme 1. Preparation of **3**.

Metal dithiocarbamate complexes show a characteristic IR band in the region 1450–1550 cm^{-1}, which has been assigned to a partially double C–N bond (thioureide bond).[9] The IR spectrum of **3** showed a marked high-frequency shift ($\Delta\tilde{\nu}$ = 96 cm^{-1}) of the signal of the C–N stretch with respect to the uncomplexed ligand **2**. Such a feature is commonly observed for the formation of dithiocarbamate complexes.[9] The ^1H NMR spectrum showed three methylene peaks which were successfully assigned by means of HETCOR and HOMCOR techniques (Figure 1). The FAB-MS spectrum displayed a set of peaks that corresponded to the parent molecule and its fragment (see Experimental Section).

Electrochemistry of nickel(II) dithiocarbamate bearing two ferrocenyl subunits (3): The capability of dithiocarbamate ligands to favor access to unusually high oxidation states is well documented.[10] In particular, studies on the irreversible oxidation–reduction process of the nickel(II) dithiocarbamate subunit have been reported[11] in which a series of dialkyldithiocarbamate complexes were used. The products from the oxidation of nickel(II) diethyldithiocarbamate $[Ni^{II}(Et_2dtc)_2]$ have been characterized and the overall process has been shown to be $3[Ni(Et_2dtc)_2] \rightarrow 2[Ni^{IV}(Et_2dtc)_3]^+ + Ni^{2+} + 4e^-$.[11] As to the complex **3**, the initial oxidation wave labeled peak **I** in Figure 2b (dotted line) is irreversible with a complex electrode process involving a ligand exchange reaction. Analogy to $[Ni(Et_2dtc)_2]$ and the following experimental facts on **3** establish the stoichiometry and the products of the oxidation to be a nickel(IV) complex bearing three ferrocenyl subunits [Eq. (1)].

$$3[Ni^{II}(Fe^{II})_2] \rightarrow 2[Ni^{IV}(Fe^{II})_3]^+ + Ni^{2+} + 4e^- \quad (1)$$

Figure 2a shows the UV/Vis spectroelectrochemical oxidation and reduction of **3**. Spectrophotometric monitoring of the initial oxidation at peak **I** showed progressive development of a broad peak at 500 nm assigned to nickel(IV)[11] at the expense of the parent Ni^{II} species ($[Ni^{II}(Fe^{II})_2]$, λ_{max} = 325, 390 nm). Controlled potential coulometry at 0.5 V afforded the non-integral n value of 1.3 electrons per mole of **3**. The nickel dithiocarbamate complex bearing three ferrocenyl groups was

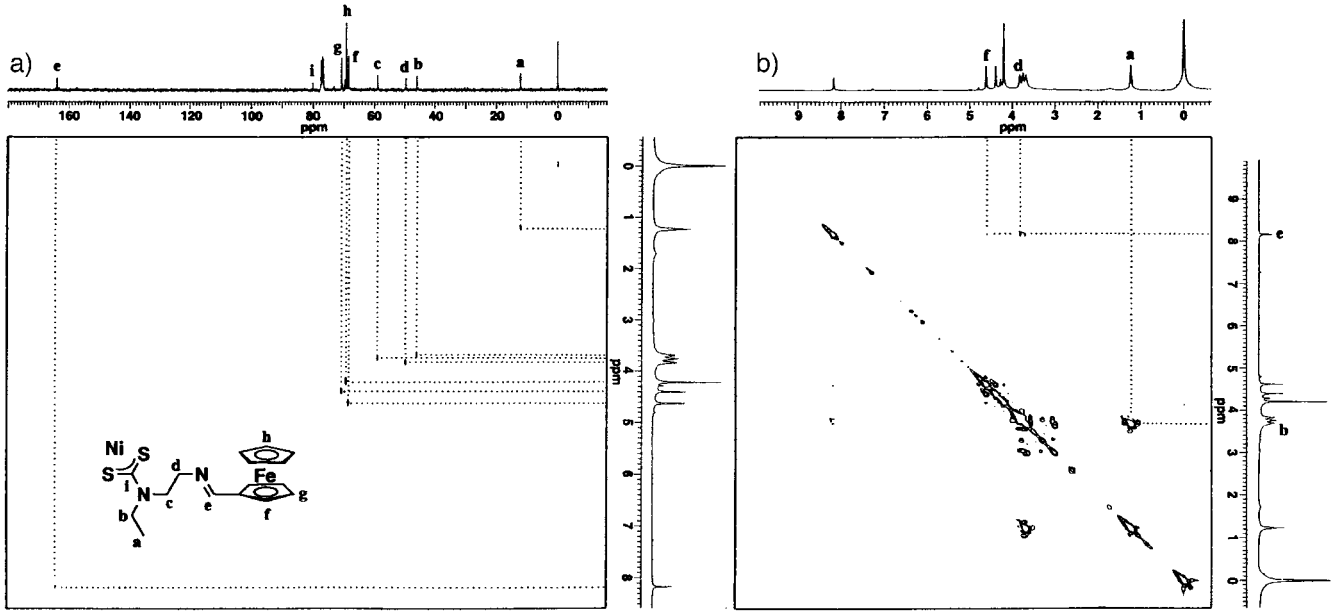

Figure 1. 270 MHz HETCOR (a) and HOMCOR (b) of **3** in $CDCl_3$.

0947-6539/99/0511-3194 $ 17.50+.50/0 *Chem. Eur. J.* **1999**, *5*, No. 11

found in the electrolyzed solution by FAB mass spectrometry (*m/z* 1137). In addition, the cyclic voltammogram developed an irreversible reduction wave at $E_{pc} = -0.40$ V (peak **IV** in Figure 2b), as observed for the irreversible reduction of $[Ni(Et_2dtc)_3]^+$ ($[Ni^{IV}(Et_2dtc)_3]^+ + e^- \rightarrow [Ni^{II}(Et_2dtc)_2] + \frac{1}{2}Et_4$-tds, where $Et_4tds = Et_2NCS_2S_2CNEt_2$ (thiuram disulfide)).[11] Indeed, spectroelectrochemistry measurements (Figure 2a) revealed that reduction at potentials more negative than -0.4 V produced the parent $Ni^{II}(Fe^{II})_2$ complex **3** [Eq. (2)].

$$[Ni^{IV}(Fe^{II})_3]^+ + e^- \rightarrow [Ni^{II}(Fe^{II})_2] + \tfrac{1}{2}(Fe)_2tds \quad (2)$$

The wave **I** substantially disappears after the first scan and a cyclic voltammogram scanned continuously between 0 and 1.4 V converges onto a steady-state curve as shown in Figure 2b (solid line). The curve corresponds to the redox behavior of the nickel(IV) complex bearing three ferrocenyl subunits and reveals a two-wave profile, labeled **II** and **III**. Controlled potential electrolysis of **3** at 0.8 and 1.1 V resulted in transfers of 0.66 and 2 electrons, respectively, per mole of total nickel, which corresponded to 1 and 3 electrons per mole of the electrogenerated nickel(IV) complex. Spectroelectrochemistry at potentials more positive than 0.6 V revealed that oxidations at **II** and **III** gave rise to a broad band near 480 nm (LMCT) and a shoulder at 260 nm due to the ferrocenium moiety (Figure 2a). Accordingly, the waves **II** and **III** are both to be assigned to the redox process of the three ferrocenyl subunits.

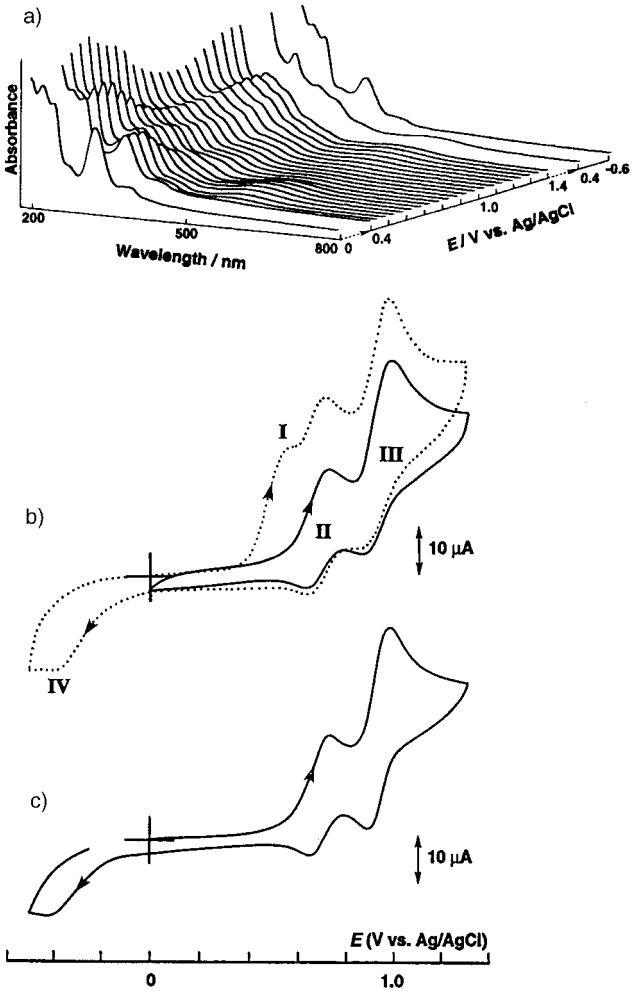

Figure 2. a) UV/Vis spectral changes during the spectroelectrochemical oxidation and reduction of **3** in CH_3CN. The supporting electrolyte contained 0.1 mol L^{-1} tetrabutylammonium tetrafluoroborate. b) Cyclic voltammograms for a 0.5 mmol L^{-1} solution of **3** in anaerobic anhydrous CH_3CN. Dotted line, first scan; solid line, steady state. Scan rate = 100 mV s^{-1}. A 6 mm diameter glassy carbon electrode was used. c) Cyclic voltammogram for a 0.33 mmol L^{-1} solution of $[\mathbf{4}^+]BF_4^-$. Other conditions were as in (b).

Added support for the coulometric titration experiments have been provided by rotating disk voltammetry. The current-potential curve in Figure 3a exhibits three waves which correspond to the three oxidation peaks **I**, **II**, and **III** in the cyclic voltammogram. The magnitudes of the three plateau currents have been labeled i_I, i_{II}, and i_{III} in Figure 3a.

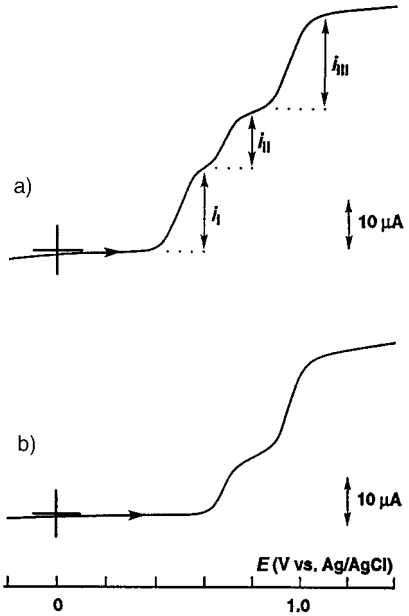

Figure 3. a) Current–potential curve recorded at a rotating disk electrode for a 0.5 mmol L^{-1}solution of **3** in anaerobic anhydrous CH_3CN. Scan rate = 5 mV s^{-1}. Electrode rotation rate = 250 rpm. A 6 mm diameter glassy carbon electrode was used. The supporting electrolyte contained 0.1 mol L^{-1} tetrabutylammonium tetrafluoroborate. b) Current–potential curve for a 0.33 mmol L^{-1} solution of $[\mathbf{4}^+]BF_4^-$. Other conditions were as in (a).

The Levich plots of each plateau current versus (electrode rotation rate)$^{1/2}$ were linear. By employing the number of electrons per mole of total nickel ($n_{app}/[Ni]_T$) for each electrode process (Table 1), the diffusion coefficients of **3** and the electrogenerated nickel(IV) complex are calculated from the magnitude of i_I and i_{II} (Table 2). A slightly smaller diffusion coefficient for the nickel(IV) complex compared to that of **3** is consistent with the increased molecular dimensions, which support the stoichiometry of the electrode process [Eq. (1)].

It is considered that because of the interactions between the iron atoms, initial one-electron oxidation at an iron site renders the subsequent oxidation of the remaining iron(II) centers energetically less favorable. Therefore subsequent oxidation occurs at a higher potential, resulting in the

Table 1. Electrochemical data for nickel complexes.[a]

Half reaction		E_{pa}[b] [V]	E_{pc}[c] [V]	$E_{1/2}$[d] [V]	$\frac{n_{app}}{[Ni]_T}$[e]
$3[Ni^{II}(Fe^{II})_2]$(**3**) $\rightarrow 2[Ni^{IV}(Fe^{II})_3]^+$ (**4**$^+$)$+Ni^{2+}+4e^-$	(**I**)	(0.55)		irrev.	1.3
$[Ni^{IV}(Fe^{II})_3]^+$ (**4**$^+$) $\rightleftharpoons [Ni^{IV}(Fe^{II})_2Fe^{III}]^{2+}$ (**4**$^{2+}$)$+e^-$	(**II**)	0.73	0.66	0.69(0.07)	0.66
$[Ni^{IV}(Fe^{II})_2Fe^{III}]^{2+}$ (**4**$^{2+}$) $\rightleftharpoons [Ni^{IV}(Fe^{III})_3]^{4+}$ (**4**$^{4+}$) $+2e^-$	(**III**)	0.99	0.89	0.94(0.1)	1.3
$[Ni^{IV}(Fe^{II})_3]^+$ (**4**$^+$)$+e^- \rightarrow [Ni^{II}(Fe^{II})_2]+$½$Fe_2$tds	(**IV**)		-0.40	irrev.	0.66
$3[Ni^{II}(Et_2dtc)_2]$[f] $\rightarrow 2[Ni^{IV}(Et_2dtc)_3]^+ + Ni^{2+}+4e^-$		(0.62)		irrev.	1.3
$[Ni^{IV}(Et_2dtc)_3]^+ + e^- \rightarrow [Ni^{II}(Et_2dtc)_2] + Et_4tds$[g]			0.13	irrev.	0.66

[a] Solvent = CH_3CN, supporting electrolyte = 0.1 mol L^{-1} $TBABF_4$. [b] Oxidation peak potential in V vs. Ag/AgCl determined by cyclic voltammetry. Sweep rate = 100 mV s^{-1}. Ferrocene/ferrocenium redox couple was 0.40 V vs. this Ag/AgCl. [c] Reduction peak potential. [d] $(E_{pa}+E_{pc})/2$. ΔE_p ($=E_{pa}-E_{pc}$, at 100 mV s^{-1}) given in parenthesis. [e] Number of electrons per mole of nickel. [f] Bis(diethyldithiocarbamato)nickel(II). Data from reference [11]. [g] $Et_2NCS_2S_2CNEt_2$, thiuram disulfide.[11]

Table 2. Diffusion coefficients of nickel complexes in CH_3CN.[a]

Complex	Abbreviation	$10^6 D$ [$cm^2 s^{-1}$][b]
3	$[Ni^{II}(Fe^{II})_2]$	3.6
4$^+$	$[Ni^{IV}(Fe^{II})_3]^+$	3.4
4^{2+}	$[Ni^{IV}(Fe^{II})_2Fe^{III}]^{2+}$	3.3
$[Ni(Et_2dtc)_2]$[c]	Ni^{II}	8.2

[a] Diffusion coefficient measured in 0.1M tetrabutylammonium tetrafluoroborate in CH_3CN. [b] Determined by Levich plots $\{i/(0.62(n_{app}/[Ni]_T)FA\omega^{1/2}\nu^{-1/6}[Ni]_T)\}^{3/2}$. $n_{app}/[Ni]_T$ is from Table 1. [c] Bis(diethyldithiocarbamato)nickel(II).

stepwise current-potential curve in Figure 3a. However, this pattern of redox coupling does not hold for the further two-electron oxidation process at **III** (Figure 2b). The peak-to-peak separation for **III** was 100 mV, and in the rotating disk voltammogram (Figure 3a) the plots of $\ln[i_{III}-\{i-(i_I+i_{II})\}/\{i-(i_I+i_{II})\}]$ versus E at $E>0.8$ V produced a straight line whose slope corresponded to one-electron transfer,[12] suggesting that two unresolved one-electron processes were responsible. Hence we could say that the two one-electron couples occur at very similar potentials at **III**. Thus the redox behavior of the nickel(IV) complex bearing three ferrocenyl subunits can be summarized as follows [Eq. (3) and (4)]:

$$[Ni^{IV}(Fe^{II})_3]^+ \rightleftharpoons [Ni^{IV}(Fe^{II})_2Fe^{III}]^{2+}+e^- \quad (3)$$

$$[Ni^{IV}(Fe^{II})_2Fe^{III}]^{2+} \rightleftharpoons [Ni^{IV}(Fe^{III})_3]^{4+}+2\,e^- \quad (4)$$

Electrochemical data for **3** and its oxidized products are summarized in Table 1.

Synthesis and electrochemistry of nickel(IV) dithiocarbamate bearing three ferrocenyl subunits ($Ni^{IV}(Fe^{II})_3]^+$) (4$^+$): Once the stoichiometry of the oxidation of **3** had been established, we then attempted to isolate the nickel(IV) complex bearing three ferrocenyl subunits. After the irreversible oxidation of **3**, the Ni^{IV} complex could be isolated from the electrolyzed solution (Scheme 2). Electrolytic oxidation of **3** in the presence of tetrabutylammonium tetrafluoroborate as a supporting electrolyte by the use of a large-area carbon-felt electrode maintained at 0.5 V consumed 1.3 ± 0.2 electrons per molecule of **3** dissolved in the initial solution, and the resulting nickel(IV) complex [**4**$^+$]BF_4^- precipitated from the electrolyzed solution upon cooling. The product, analytically pure in 35% yield, was identified by spectroscopic methods and elemental analysis (see Experimental Section).

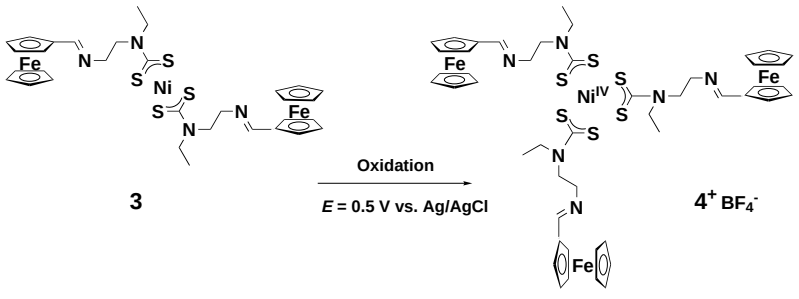

Scheme 2. Preparation of [**4**$^+$]BF_4^-.

The cyclic voltammogram obtained for a solution prepared by dissolving the isolated complex [**4**$^+$]BF_4^- in CH_3CN is shown in Figure 2c. The voltammogram, with two quasireversible waves at 0.69 and 0.94 V, is identical to the steady-state curve obtained for **3** (Figure 2b, solid line). Figure 3b shows a current-potential curve for **4**$^+$ recorded at a rotating disk electrode. The lack of anodic current at 0.5 V reflects the absence of the nickel(II) center. The two waves are assigned to the oxidations of the three ferrocenyl centers according to the reactions in Equations (3) and (4), and are consistent with the results observed for the nickel(IV) complex electrochemically generated in situ from **3**.

Synthesis and electrochemistry of model complexes: To examine the effect that nickel(IV) center has on the redox properties of **4**$^+$, ferrocenylimine **5** and bisferrocenylimine **6** were synthesized as model compounds according to Scheme 3 by means of C=N bond formation upon the reaction of ferrocenecarboxaldehyde and primary amine nucleophiles.

Figure 4a shows the cyclic voltammogram of **5**. The wave is quasireversible ($i_{pc}/i_{pa}=0.8$ at a scan rate of 100 mV s^{-1} where i_{pa} and i_{pc} are anodic and cathodic peak currents in cyclic voltammetry) which compare well with that of **4**$^+$ ($i_{pc}/i_{pa}=0.7$ (**II**) and 0.8 (**III**) at 100 mV s^{-1} (Figure 2c)). Controlled potential coulometry at 0.8 V afforded the n value of 1 ± 0.1 electron per mole of **5**. Like ferrocene itself, the complex **5** undergoes one-electron oxidation to the corresponding ferrocenium. The half-wave potential of **5** determined by cyclic voltammetry is given in Table 3. The ferrocenyl subunits in **4**$^+$,

0947-6539/99/0511-3196 $ 17.50+.50/0 *Chem. Eur. J.* **1999**, *5*, No. 11

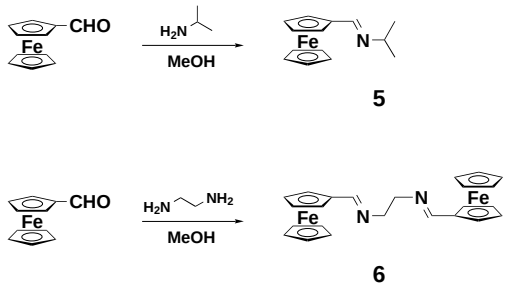

Scheme 3. Preparation of **5** and **6**.

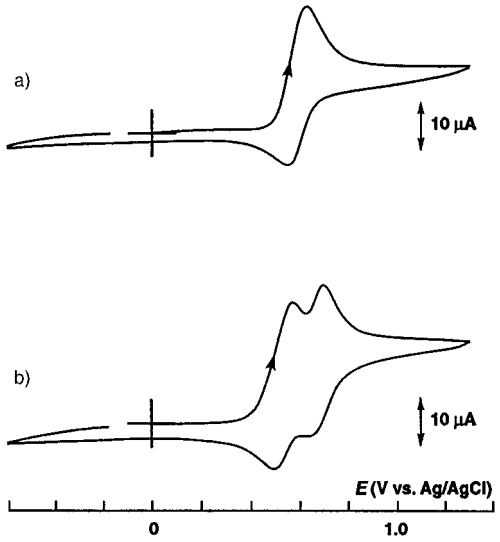

Figure 4. a) Cyclic voltammogram for a 0.5 mmol L^{-1} solution of **5** in anaerobic anhydrous CH_3CN. Scan rate = 100 mV s^{-1}. A 6 mm diameter glassy carbon electrode was used. The supporting electrolyte contained 0.1 mol L^{-1} tetrabutylammonium tetrafluoroborate. b) Cyclic voltammogram for a 0.5 mmol L^{-1} solution of **6**. Other conditions were as in (a).

Table 3. Electrochemical data for ferrocenylimines.[a]

Half reaction	E_{pa}[b] [V]	E_{pc}[c] [V]	$E_{1/2}$[d] [V]	n_{app}[e] / $[Fe]_T$
$[Fe^{II}]$ (**5**) $\rightleftharpoons$ $[Fe^{III}]^+$ (**5**$^+$)+e^-	0.64	0.54	0.59 (0.1)	1
$[(Fe^{II})_2]$ (**6**) $\rightleftharpoons$ $[Fe^{II}Fe^{III}]^+$ (**6**$^+$)+e^-	0.57	0.50	0.54 (0.07)	0.5
$[Fe^{II}Fe^{III}]^+$ (**6**$^+$) $\rightarrow$ $[(Fe^{III})_2]^{2+}$ (**6**$^{2+}$)+e^-	0.70	0.64	0.67 (0.06)	0.5

[a] Solvent = CH_3CN, supporting electrolyte = 0.1 mol L^{-1} $TBABF_4$. [b] Oxidation peak potential in V vs. Ag/AgCl determined by cyclic voltammetry. Sweep rate = 100 mV s^{-1}. Ferrocene/ferrocenium redox couple was 0.40 V vs. this Ag/AgCl. [c] Reduction peak potential. [d] $(E_{pa}+E_{pc})/2$. ΔE_p $(= E_{pa} - E_{pc}$, at 100 mV $s^{-1})$ given in parenthesis. [e] Number of electrons per mole of iron.

with an appended nickel(IV) center, induce a slight increase in the initial oxidation potential compared to the ferrocenylimine **5** as a result of an electron-withdrawing effect propagated through the dithiocarbamate moiety and/or an electrostatic effect which reflect the local solvation mode that can be influenced by the +1 charge on the nickel(IV) dithiocarbamate center.

Biferrocenes generally undergo reversible one-electron oxidations with the number of waves determined by the number of ferrocenyl units. The complex **6** undergoes two successive quasireversible one-electron oxidations to yield the mono- and dications. Controlled potential electrolysis at 0.5 and 0.8 V consumed 1.0 ± 0.1 and 2.0 ± 0.2 electrons, per mole of **6**. The well-resolved one-electron waves in cyclic voltammetry (Figure 4b) allowed assignment of peak potentials as summarized in Table 3.

Comproportionation equilibria: The intriguing aspect of the redox behavior of the complex **4**$^+$ is the significant redox coupling between three ferrocenyl subunits, as evidenced by the electrochemical data. An estimate for the extent of the ferrocene–ferrocene interactions is obtained from the value of the comproportionation constants, $K_c(5)$ and $K_c(6)$, for equilibria (5) and (6), respectively.

$$[Ni^{IV}(Fe^{II})_3]^+ + [Ni^{IV}(Fe^{III})_2Fe^{II}]^{3+} \rightleftharpoons 2\,[Ni^{IV}Fe^{III}(Fe^{II})_2]^{2+}; K_c(5) \quad (5)$$

$$[Ni^{IV}Fe^{III}(Fe^{II})_2]^{2+} + [Ni^{IV}(Fe^{III})_3]^{4+} \rightleftharpoons 2\,[Ni^{IV}(Fe^{III})_2Fe^{II}]^{3+};\ K_c(6) \quad (6)$$

For oxidations of ferrocenyl subunits, the waves labeled **II** and **III** are well resolved by cyclic voltammetry (Figures 2b and c). The value of $K_c(5)$ is related to the extent of redox coupling; the separation between the two consecutive redox potentials $\Delta E^f = E^f(\mathbf{III}) - E^f(\mathbf{II})$, by the expression $\ln K_c(5) = F\Delta E^f/RT$. The value of $\Delta E_{1/2} = E_{1/2}(\mathbf{III}) - E_{1/2}(\mathbf{II})$, due to the electrochemically quasireversible nature of the process, approximates ΔE^f. The obtained value of $\Delta E_{1/2}$ of 250 mV corresponds to a $K_c(5)$ value of 1.7×10^4. On the other hand, the absence of redox coupling at the wave **III** containing two superimposed one-electron transfers at the two electrochemically equivalent ferrocenyl subunits suggests that $K_c(6)$ is significantly smaller than $K_c(5)$. The relatively low resolution of electrochemical techniques means that accurate determination of K_c values smaller than about 33 (corresponding to a ΔE^f value of ca. 90 mV) are difficult. However, one could say that $K_c(6)$ is much closer to the statistical limit $(33 > K_c(6) \approx 4)$ than $K_c(5)$.

For various mixed-valence biferrocenes bridged by sp^3 carbons, no intervalence transfer transition has been observed in the near-infrared region. Such compounds are characterized by the small redox coupling: the electrochemistry of a series of dicopper complexes with *N,N*-linked bis(cyclam) ligands has been reported by Fabbrizzi et al[13] in which the redox coupling was 115 mV for a $-(CH_2)_2-$ bridge, 80 mV for a $-(CH_2)_3-$ bridge, and 54 mV for a $-(CH_2)_4-$ bridge. The value for the model complex, bisferrocenylimine **6**, is 130 mV (Table 3) which is comparable to that of the dicopper complex with the ethylene-bridged bis(cyclam) ligands.[13] Surprisingly, the ferrocenyl subunits bridged by the nickel(IV) center in **4**$^+$ showed a substantially larger value (250 mV) of redox coupling. Considering that the resonance forms of the ligand **2** as depicted in Scheme 4 indicate that four sp^3 carbons are involved between ferrocenyl subunits in **4**$^+$ and hence no low-energy transition due to intervalence electron delocalization

Scheme 4. Resonance forms for the ferronenyldithiocarbamate ligand **2**.

is found, one could safely state that the significant deviation of $K_c(5)$ with respect to the statistical limit is due to the electrostatic interaction between the ferrocenyl groups.[14] The value of $K_c(5)$ indicates that the mixed-valence state $[Ni^{IV}Fe^{III}(Fe^{II})_2]^{2+}$ ($\mathbf{4}^{2+}$) substantially persists in solution. However, attempts to isolate the $[Ni^{IV}Fe^{III}(Fe^{II})_2]^{2+}$ complex from the electrolyzed solution of $\mathbf{4}^+$ at 0.8 V failed because of the difficulties in the isolation of molecules that display electrochemical quasireversibility by the bulk electrolysis method.

Preliminary force-field simulations: conformations and energetics: Two questions may arise: 1) Why are $K_c(5)$ and $K_c(6)$ so different? 2) Why is $K_c(5)$ so large? A tentative explanation is provided by consideration of the estimated molecular structures of $\mathbf{4}^+$ and its oxidized products as follows. Although the crystal structures of $[Ni(Et_2dtc)_2]$,[15] $[Ni\{(nBu)_2dtc\}_3]Br$[11] and ferrocene[16] are known, X-ray analyses of **3** and its electrooxidized product $\mathbf{4}^+$ were unsuccessful. Reasoning that crystallization might be disfavored because of the flexibility of the ethylene groups in the molecule, we turned to structure estimation by force-field calculations. Figure 5 shows the

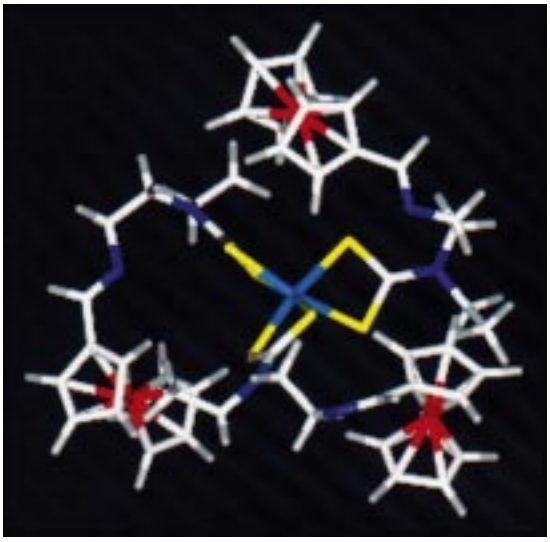

Figure 5. A perspective view of the energy-minimized conformation of $\mathbf{4}^+$ obtained by repeated force-field minimization and annealing dynamics simulations projected along the approximate C_3 axis passing through the central nickel(IV): Ni (blue), Fe (red), C (white), H (gray), S (yellow), N (purple).

energy-minimized conformation of $\mathbf{4}^+$ obtained by repeated force-field minimization and annealing dynamics calculations. A favorable *cisoid* conformation of the ethylene bridge makes the molecule approximately C_3 symmetric. Figure 6 shows the snapshots of $\mathbf{4}^+$ and its oxidized molecules which are equilibrated at 298 K during molecular dynamics simulation. It was confirmed that, during the calculations, no significant divergence from the C_3 symmetric conformation is produced which could cause the splitting in the redox waves. However, one could note that molecular dimensions are larger at higher oxidation states. The question arises what sort of energy causes the total energy decrease in the dimensional increment. By dividing the total energy, we have determined that the energy decrease is mainly caused by the electrostatic effect. This tendency is clearly indicated in Figure 7 which shows plots of mean Fe–Fe distance versus Coulomb energy of the molecule over the time at which each oxidation state was maintained at 298 K during simulation. The Coulomb energy is calculated at a unit dielectric constant. Except for $\mathbf{4}^+$, the Coulomb energies have negative hyperbolic dependence on the mean Fe–Fe distances. The Coulomb energy in $\mathbf{4}^+$ is almost independent of the molecular geometry because of the absence of electrostatic repulsion between the neutral subunits. When at least one of the three ferrocenyl subunits is oxidized on the contrary, the Coulomb energy becomes geometry-dependent due to the repulsion between the oxidized ferrocenyl subunits and the nickel(IV) center, both bearing +1 charge.

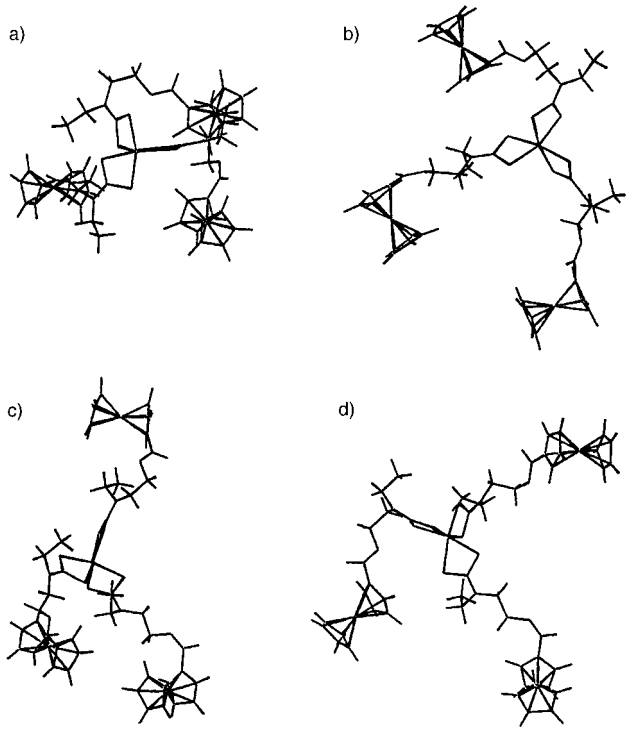

Figure 6. Snapshots of a) $[Ni^{IV}(Fe^{II})_3]^+$ ($\mathbf{4}^+$), b) $[Ni^{IV}Fe^{III}(Fe^{II})_2]^{2+}$ ($\mathbf{4}^{2+}$), c) $[Ni^{IV}Fe^{II}(Fe^{III})_2]^{3+}$ ($\mathbf{4}^{3+}$), and d) $[Ni^{IV}(Fe^{III})_3]^{4+}$ ($\mathbf{4}^{4+}$) during the molecular dynamics simulations at 298 K. The dielectric value was set at 1.0. The structural parameters of the N-CS_2 group were fixed at the value of the crystal structure of nickel(II) diethyldithiocarbamate[15] so that conformational changes were mainly caused by the free rotations around C–C and C–N bonds.

The free energy change ΔG_c^0 associated with the comproportionation equilibrium is related to the extent of redox coupling according to $\Delta G_c^0 = -nF\Delta E^0$. The electrostatic repulsion term ΔG_e^0 is defined as a deviation of ΔG_c^0 from the statistical fixed term ($-$RT ln4) according to $\Delta G_e^0 = \Delta G_c^0 + RT\ln 4$. The electrostatic contribution, ΔG_e^0, reflects the decrease in the electrostatic repulsion between metal centers which occurs during the comproportionation process. Many attempts have been made, for example by the use of the complexes with N,N-linked bis(cyclam) ligands quoted above,[13] to formulate ΔG_e^0 by the equation $\Delta G_e^0 \propto 1/Dr$ where D is the dielectric constant of the medium and r is the

0947-6539/99/0511-3198 $ 17.50+.50/0 *Chem. Eur. J.* **1999**, *5*, No. 11

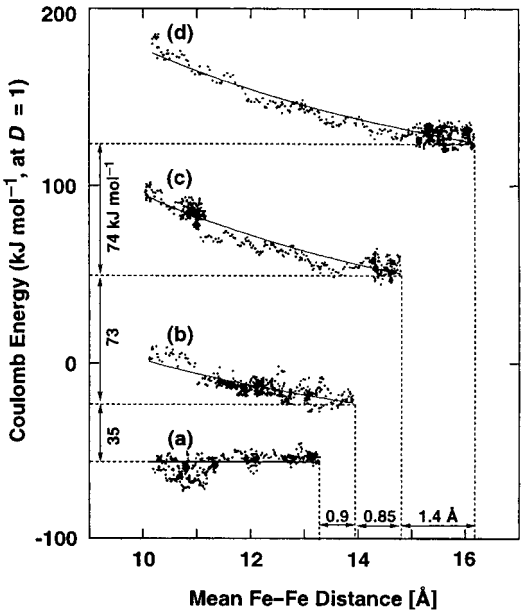

Figure 7. The parametric plots between the mean Fe–Fe distance and the Coulomb energy at a unit dielectric value during the molecular dynamics simulations at 298 K: a) $[Ni^{IV}(Fe^{II})_3]^+$ ($\mathbf{4}^+$), b) $[Ni^{IV}Fe^{III}(Fe^{II})_2]^{2+}$ ($\mathbf{4}^{2+}$), c) $[Ni^{IV}Fe^{II}(Fe^{III})_2]^{3+}$ ($\mathbf{4}^{3+}$), and d) $[Ni^{IV}(Fe^{III})_3]^{4+}$ ($\mathbf{4}^{4+}$). The solid line in a) represents an arithmetic mean value of the Coulomb energies. The solid lines in b), c), and d) represent the least-squares fitted curves according to the hyperbolic equation ($y = a/x + b$) which correspond to the energy profiles along the mean Fe–Fe distances describing the relaxation upon dimensional increase in the molecules.

distance between the metal centers.[17] In previous studies on the decay law of the metal–metal coupling with distance, it has been considered that r is not dramatically changed ($\Delta <$ 0.1 Å) upon oxidation,[18] so that isostructural sets of dinuclear complexes with different metal–metal distances have frequently been synthesized and employed to estimate the metal–metal interaction. In contrast, our preliminary molecular dynamics simulations have revealed that the oxidation process of the ferrocenyl subunit in $\mathbf{4}^+$ [Eq. (3)] results in a considerable increment in molecular dimensions because of the electrostatic repulsion between the appended sites. Here we do not intend to provide the decay law for Fe–Fe coupling, but attempt to show that structural dynamics associated with electron transfer is responsible for the characteristic electrochemical behavior. Figure 7 shows that, upon oxidation, the mean Fe–Fe distance (r_{Fe-Fe}) becomes significantly larger at each relaxed state ($\Delta r_{Fe-Fe} = 0.9$ Å ($\mathbf{4}^+/\mathbf{4}^{2+}$), 0.85 Å ($\mathbf{4}^{2+}/\mathbf{4}^{3+}$), 1.4 Å ($\mathbf{4}^{3+}/\mathbf{4}^{4+}$)). The diffusion coefficient of $\mathbf{4}^{2+}$, which is slightly smaller than that of $\mathbf{4}^+$ (Table 2), could reflect the increased molecular dimensions. It can be reasoned that such an increase in r_{Fe-Fe} (i.e. decrease in Coulomb energy) which accompanies the comproportionation reaction (5) affords ΔG_e^0, while the energetics in reaction (6) are dominated mainly by the statistical term allowing two one-electron transfers [Eq (4)] to occur at very similar potentials. Thus the difference in $K_c(5)$ and $K_c(6)$ stems from the marked contrast of the energy profile of $\mathbf{4}^+$ (independent of r_{Fe-Fe}) to those of $\mathbf{4}^{2+}$, $\mathbf{4}^{3+}$, and $\mathbf{4}^{4+}$. Comparisons between the energy profiles provide approximate values of the decrease in Coulomb energy with reactions (5) and (6) at a unit dielectric constant. The value of $D\Delta G_e^0$ calculated for reaction (5) ($-73 + 35 = -38$ kJ mol^{-1}) is much larger than that for reaction (6) ($-74 + 73 = -1$ kJ mol^{-1}). Since the experimentally determined value is $\Delta G_e^0 = -nF\Delta E_{1/2} + RT \ln 4 = -20.7$ kJ mol^{-1}, the local dielectric constant D is evaluated to be 1.9, which is much lower than that of the bulk solvent (38.8 at 25 °C). It has been shown[13, 19] that bulk values of D are absolutely not appropriate to describe short-range phenomena, and individual values of D that reflect the local solvation mode should be used. The interpretation is forcibly qualitative since we are not in the position to quantify the local dielectric value. Simulations of the nickel(IV) complex with the ferrocenyl subunits immersed in explicit acetonitrile molecules are the subject of our continuing investigation.

Finally, it would be interesting to compare the results on energetics of $\mathbf{4}^+$ with that of **6**. Preliminary molecular dynamics simulations on **6** have been carried out under the similar conditions. The Coulomb energy changes that accompany the comproportionation reaction ($[(Fe^{II})_2]$ (**6**) + $[(Fe^{III})_2]^{2+}$ ($\mathbf{6}^{2+}$) $\rightleftharpoons 2[Fe^{II}Fe^{III}]^+$ ($\mathbf{6}^+$)) are found to be consistent with the electrochemical data ($D\Delta G_e^0 \ll 0$) but the geometric parameters are almost independent of the oxidation state in contrast to the result for $\mathbf{4}^+$. This is because in the simulation of **6**, the ethylene bridge does not undergo such a large conformational change as observed in the simulation of $\mathbf{4}^{n+}$. In addition, the electrostatic effect in $\mathbf{4}^{n+}$ also appears to reflect the +1 charge on the nickel(IV) dithiocarbamate center which could affect the local dielectric constant. We did not employ molecular dynamics calculation techniques with a view to obtain the absolute values of ΔG_e^0 associated with comproportionation reactions, but to compare the energetics of isostructural molecules in different oxidation states. However, it is noteworthy that two molecular dynamics simulations with different molecules ($\mathbf{4}^+$ and **6**) provided a similar predictions concerning the approximate energy changes associated with the comproportionation reactions of redox states.

Conclusions

We have attempted to interpret the electrochemical behavior of species containing three chemically equivalent ferrocenyl groups according to an electrostatic model. Preliminary results have shown that conformational dynamics associated with an electron transfer is responsible for the entire electrochemical behavior of the molecule which exchanges three electrons in two steps. For the quantitative description of the electrostatic interaction, local dielectric constants need to be employed to evaluate the shielding effect exerted by the solvational molecules, which may be much less than the bulk value. It is surprising to note that in spite of the long bridging aliphatic chains, the two ferrocenyl subunits in $\mathbf{4}^+$ interact considerably. This property renders the ligand **2** of interest as a possible component to aid communication through various metal centers.

Experimental Section

Materials: All solvents were purified by distillation. Tetrabutylammonium tetrafluoroborate was obtained from Wako Chem. Co. and recrystallized

from the mixture of benzene and ethyl acetate. Ferrocenecarboxaldehyde, *N*-ethylethylenediamine, potassium hydroxide, carbon disulfide, nickel(II) chloride, isopropylamine, ethylenediamine, and nickel(II) dietyldithiocarbamate were obtained from Kanto Chem. Co. and used without further purification.

Measurements: All measurements were performed in a dry box under an atmosphere of dry argon. Electrochemical measurements were carried out in a conventional two-compartment cell. A glassy carbon disk was used as a working electrode and polished before each experiment with 0.05 μm alumina paste. The auxiliary electrode, a coiled platinum wire, was separated from the working solution by a fine-porosity frit. The reference electrode was a commercial Ag/AgCl electrode immersed in a salt bridge consisting of 0.1 mol L^{-1} tetrabutylammonium tetrafluoroborate, which was placed in a main cell compartment. The formal potential of the ferrocene/ferrocenium couple in dichloromethane was 0.40 V vs. this reference electrode. All potentials are quoted with respect to this Ag/AgCl reference electrode. A Nikko Keisoku DPGS-1 dual potentiogalvanostat and a Nikko Keisoku NFG-3 universal programmer were employed with a Graphtec WX2400 X-Y recorder to obtain the voltammograms. Coulometric exhaustive electrolysis was performed with a Nikko Keisoku NDCM-1 digital coulometer. UV/Vis spectra were obtained with a Shimadzu UV-2100 spectrophotometer. A platinum mesh working electrode and a quartz glass cell with optical path length of 2 mm were used for spectroelectrochemical measurements. Infrared spectra were obtained with a JASCO FT-IR 5300 as potassium bromide pellets. FABMS spectrum was obtained on a VGZAB-HF spectrometer with *m*-nitrobenzyl alcohol as the matrix material. HETCOR and HOMCOR spectra were obtained on a JEOL 270 MHz GSX270 NMR spectrometer.

Synthetic procedures: Synthetic routes to the ferrocene-tethered nickel(II) (**3**) and nickel(IV) (**4**) complexes are shown in Schemes 1 and 2. Ferrocenecarboxaldehydeisopropylimine (**5**) and bis(ferrocenecarboxaldehyde)ethylenediimine (**6**) were synthesized by conventional methods as shown in Scheme 3.

Ligand 2: All procedures were performed under nitrogen atmosphere in the dark. To a solution of ferrocenecarboxaldehyde (5.35 g, 2.5×10^{-2} mol) in anhydrous methanol (100 mL) was added dropwise *N*-ethylethylenediamine (2.2 g, 2.5×10^{-2} mol). Schiff-base formation was monitored by the disappearance of the ν(C=O) band of the aldehyde at 1680 cm^{-1} in the IR spectra and the subsequent appearance of the ν(C=N) band at 1640 cm^{-1}. The mixture was evaporated and the resulting orange-red solid was dried under vacuum to give **1**. To a suspension of **1** in H_2O (200 mL) held at 0 °C was added potassium hydroxide (1.41 g, 2.5×10^{-2} mol) and carbon disulfide (1.90 g, 2.5×10^{-2} mol). The mixture was stirred at 0 °C overnight, evaporated and dried under vacuum to give **2** as a dark brown powder. IR (KBr): $\tilde{\nu} = 1639$ (C=N), 1506 cm^{-1} (C–N); ^{1}H NMR (270 MHz, $CDCl_3$, 25 °C, TMS): $\delta = 1.20$ (t, 3H; CH_3), 3.63 (m, 6H; CH_2), 4.29 (s, 5H; C_5H_5), 4.60 (d, 2H; C_5H_4), 4.80 (d, 2H; C_5H_4), 8.46 (s, 1H; CH=N); MS (70 eV): *m/z*: 283 ($[M^+ - CS_2K]$); elemental analysis (%) calcd for $C_{16}H_{19}FeKN_2S_2$: C 48.23, H 4.81, N 7.03; found C 48.01, H 4.79, N 7.01.

Nickel(II) dithiocarbamate bearing two ferrocenyl subunits (3): The nickel(II) complex **3** was prepared from nickel(II) chloride and **2** as follows. To a filtrate of **2** (0.38 g, 1×10^{-3} mol) in H_2O (100 mL) was added dropwise a solution of nickel chloride (0.06 g, 0.2×10^{-3} mol) in H_2O (10 mL). The resulting green precipitate was collected by filtration, washed thoroughly with H_2O and dried under vacuum to give **3**. IR (KBr): $\tilde{\nu} = 1639$ (C=N), 1506 (C–N), 1128 (C–S), 1086 cm^{-1} (N–C2); ^{1}H NMR (270 MHz, $CDCl_3$, 25 °C, TMS): $\delta = 1.23$ (t, $^3J = 7$ Hz, 6H; CH_3), 3.69 (q, $^3J = 7$ Hz, 4H; CH_2), 3.75 (t, $^3J = 7$ Hz, 4H; CH_2), 3.83 (t, $^3J = 7$ Hz, 4H; CH_2), 4.21 (s, 10H; C_5H_5), 4.40 (d, $^3J = 6$ Hz, 4H; C_5H_4), 4.62 (d, $^3J = 6$ Hz, 4H; C_5H_4), 8.17 (s, 2H; CH=N); ^{13}C NMR ($CDCl_3$, 25 °C, TMS): $\delta = 12.18$ (CH_3), 45.96 (CH_2), 49.62 (CH_2), 58.91 (CH_2), 68.43 (C_5H_4), 69.18 (C_5H_5), 69.66 (C_5H_4), 70.67 (C_5H_4), 80.03 (CS_2), 163.81 (C=N); MS (70 eV): *m/z*: 777 ($[M^+]$), 580 ($[M - C(C_{10}H_9Fe)]$), 327, 295; UV (CH_3CN): $\lambda_{max} = 325$, 390 nm; elemental analysis (%) calcd for $C_{32}H_{38}Fe_2N_4NiS_4$: C 49.45, H 4.93, N 7.21; found: C 49.57, H 4.90, N 7.23.

Nickel(IV) dithiocarbamate bearing three ferrocenyl subunits $[4^+]BF_4^-$: The nickel(IV) complex 4^+ was prepared by the electrooxidation of **3** as follows. The nickel(II) complex **3** (0.19 g, 2.5×10^{-4} mol) was dissolved in acetonitrile (25 mL) containing tetrabutylammonium tetrafluoroborate (0.41 g, 1.25×10^{-3} mol) as a supporting electrolyte. Electrolysis of the solution was performed by using a large-area carbon-felt working electrode, a platinum coiled wire as a counter electrode, an Ag/AgCl reference electrode and a conventional two-compartment electrochemical cell. The potential of the working electrode was kept at 0.5 V throughout electrolysis, which consumed 1.31 electrons per total amount of nickel dissolved in the solution. After electrolysis, the resulting solution was cooled to −20 °C, which resulted in slow precipitation of $[4^+]BF_4^-$ as a brown powder. Analytically pure complex was successfully isolated after washing the powder thoroughly with H_2O. IR (KBr): $\tilde{\nu} = 1638$ (C=N), 1505 (C–N), 1505 (C–N), 1128 (C–S), 1090 (N–C2), 1080 cm^{-1} (BF_4); ^{1}H NMR (270 MHz, $CDCl_3$, 25 °C, TMS): $\delta = 1.22$ (t, 9H; CH_3), 3.6–3.9 (m, 18H; CH_2), 4.22 (s, 15H; C_5H_5), 4.39 (d, 6H; C_5H_4), 4.63 (d, 6H; C_5H_4), 8.17 (s, 3H; CH=N); ^{19}F NMR (400 MHz, $CDCl_3$, 25 °C, CF_3COOH ($\delta = -78$)): $\delta = -155$ (s, BF_4^-); MS (70 eV): *m/z*: 1137 ($[M^+ - BF_4]$); elemental analysis (%) calcd for $C_{48}H_{57}Fe_3N_6S_6NiBF_4$: C 47.12, H 4.70, N 6.87; found C 46.99, H 4.71, N 6.79.

Ferrocenecarboxaldehydeisopropylimine (5): To a solution of ferrocenecarboxaldehyde (1.07 g, 5.0×10^{-3} mol) in methanol (30 mL) was added dropwise a solution of isopropylamine (0.3 g, 5.0×10^{-3} mol) in methanol (20 mL). Schiff-base formation was monitored by the disappearance of the ν(C=O) band of the aldehyde at 1680 cm^{-1} in the IR spectra and the subsequent appearance of the ν(C=N) band at 1640 cm^{-1}. The mixture was evaporated and the resulting brown solid was dried under vacuum to give **5**. IR (KBr): $\tilde{\nu} = 1640$ cm^{-1} (C=N); ^{1}H NMR (270 MHz, $CDCl_3$, 25 °C, TMS): $\delta = 1.15$ (d, 6H; CH_3), 3.76 (m, 1H; CH), 4.14 (s, 5H; C_5H_5), 4.32 (s, 2H; C_5H_4), 4.61 (s, 2H; C_5H_4), 8.15 (s, 1H; CH=N); MS (70 eV): *m/z*: 255 ($[M^+]$); UV (CH_3CN): $\lambda_{max} = 273$, 450 nm; elemental analysis (%) calcd for $C_{14}H_{17}FeN$: C 62.63, H 5.13, N 6.15; found C 62.61, H 5.12, N 6.02.

Bis(ferrocenecarboxaldehyde)ethylenediimine (6): To a solution of ferrocenecarboxaldehyde (1.07 g, 5.0×10^{-3} mol) in methanol (30 mL) was added dropwise a solution of ethylenediamine (0.15 g, 2.5×10^{-3} mol) in methanol (20 mL). Schiff-base formation was monitored by the disappearance of the ν(C=O) band of the aldehyde at 1680 cm^{-1} in the IR spectra and the subsequent appearance of the ν(C=N) band at 1640 cm^{-1}. The mixture was evaporated and the resulting brown solid was dried under vacuum to **6**. IR (KBr): $\tilde{\nu} = 1640$ cm^{-1} (C=N); ^{1}H NMR (270 MHz, $CDCl_3$, 25 °C, TMS): $\delta = 3.72$ (s, 4H; CH_2), 4.12 (s, 5H; C_5H_5), 4.30 (s, 2H; C_5H_4), 4.59 (s, 2H; C_5H_4), 8.12 (s, 1H; CH=N); MS (70 eV): *m/z*: 452 ($[M^+]$); UV (CH_3CN): $\lambda_{max} = 273$ nm; elemental analysis (%) calcd for $C_{24}H_{24}Fe_2N_2$: C 65.89, H 6.73, N 5.49; found C 65.01, H 6.69, N 5.38.

Computational methods: The system we simulated consisted of the nickel(IV) cations bearing three ferrocenyl subunits 4^{n+} ($n = 1-4$). The formal charge on each Fe atom was set at either +2 or +3 according to the oxidation state, before the partial charge assignment. The initial structures for simulations were obtained by repeated energy minimization and annealing dynamics calculations (100–1000 K) using the Discover program from Molecular Simulations Inc. During calculation, structural parameters of the nickel dithiocarbamate subunit were fixed at the values from the X-ray data reported for nickel(II) diethyldithiocarbamate.[15] Since we conducted an extended simulation during which molecular dimensional changes were observed, the choice of the initial structure did not affect the results presented in this paper. We first performed a 300 step energy minimization. Then 0.01 ns molecular dynamics simulations were carried out with the initial velocities randomly assigned to realize the Boltzmann distribution at 298 K. All calculations, including the Coulomb interactions, were calculated without cutoff. The total energy of the system was conserved throughout the calculations. The dielectric value of the media was set at 1.0 (defined as distance dependent). The molecular dynamics trajectory was saved every 20 steps (20 fs interval) for subsequent analysis.

Acknowledgments

This work was partially supported by the Grant-in-Aid for Scientific Research (Nos. 09555297, 09650982 and 11650878), and the International Scientific Research Program (Joint Research No. 08044174) from the Ministry of Education, Science, Sports and Culture, Japan.

[1] a) C. Valério, J. -L. Fillaut, J. Ruiz, J. Guittard, J. -C. Blais, D. Astruc, *J. Am. Chem. Soc.* **1997**, *119*, 2588; b) J. -L. Fillaut, J. Linares, D.

  0947-6539/99/0511-3200 $ 17.50+.50/0

Astruc, *Angew. Chem.* **1994**, *106*, 2540; *Angew. Chem. Int. Ed. Engl.* **1994**, *33*, 2460.

[2] a) K. Yamamoto, K. Oyaizu, E. Tsuchida, *J. Am. Chem. Soc.* **1996**, *118*, 12665; b) K. Oyaizu, K. Yamamoto, K. Yoneda, E. Tsuchida, *Inorg. Chem.* **1996**, *35*, 6634; c) E. Tsuchida, K. Yamamoto, K. Oyaizu, N. Iwasaki, F. C. Anson, *Inorg. Chem.* **1994**, *33*, 1056; d) K. Oyaizu, E. Tsuchida, *J. Am. Chem. Soc.* **1998**, *120*, 237; e) E. Tsuchida, K. Yamamoto, K. Oyaizu, *J. Electroanal. Chem.* **1997**, *438*, 167.

[3] a) G. D. Santis, L. Fabbrizzi, M. Licchelli, C. Mangano, P. Pallavicini, A. Poggi, *Inorg. Chem.* **1993**, *32*, 854; b) L. Fabbrizzi, L. Montagna, A. Poggi, T. A. Kaden, L. Siegfried, *Inorg. Chem.* **1986**, *25*, 2671.

[4] a) I. Cuadrado, C. M. Casado, B. Alonso, M. Morán, J. Losada, V. Belsky, *J. Am. Chem. Soc.* **1997**, *119*, 7613; b) B. Alonso, M. Morán, C. M. Casado, F. Lobete, J. Losada, I. Cuadrado, *Chem. Mater.* **1995**, *7*, 1440; c) F. Ammar, J. M. Savéant, *J. Electroanal. Chem.* **1973**, *47*, 215; d) J. B. Flanagan, S. Margel, A. J. Bard, F. C. Anson, *J. Am. Chem. Soc.* **1978**, *100*, 4248; e) J. E. Sutton, P. M. Sutton, H. Taube, *Inorg. Chem.* **1979**, *18*, 1017; f) J. R. Reimers, N. S. Hush, *Inorg. Chem.* **1990**, *29*, 4510.

[5] a) D. P. Rillema, R. W. Callahan, K. B. Mack, *Inorg. Chem.* **1982**, *21*, 2589; b) D. Astruc, M. -H. Desbois, M. Lacoste, N. Ardoin, L. Toupet, F. Varret in *Mixed Valency Systems: Applications in Chemistry, Physics and Biology,* (Ed.: K. Prassides), Kluwer, Amsterdam, **1991**, pp. 107–118; c) L. O. Spreer, A. Li, D. B. MacQueen, C. B. Allan, J. W. Otvos, M. Calvin, R. B. Frankel, G. C. Papaefthymiou, *Inorg. Chem.* **1994**, *33*, 1753; d) for a recent review on intramolecular communication see S. Barlow, D. O'Hare, *Chem. Rev.* **1997**, *97*, 637.

[6] E. Gallo, E. Solari, N. Re, C. Floriani, A. Chiesi-Villa, C. Rizzoli, *J. Am. Chem. Soc.* **1997**, *119*, 5144.

[7] D. Astruc, *Acc. Chem. Res.* **1997**, *30*, 383.

[8] a) P. D. Beer, M. G. B. Drew, D. Hesek, R. Jagessar, *J. Chem. Soc. Chem. Commun.* **1995**, 1187; b) Y. Zhu, O. Clot, M. O. Wolf, G. P. A. Yap, *J. Am. Chem. Soc.* **1998**, *120*, 1812; c) N. D. Jones, M. O. Wolf, D. M. Giaquinta, *Organometallics,* **1997**, *16*, 1352; d) B. Bodenant, F. Fages, M. -H. Delville, *J. Am. Chem. Soc.* **1998**, *120*, 7511; e) P. D. Beer, J. E. Nation, S. L. W. McWhinnie, M. E. Harman, M. B. Hursthouse, M. I. Ogden, A. H. White, *J. Chem. Soc. Dalton Trans.* **1991**, 2485; f) G. Denti, S. Campagna, S. Serroni, M. Ciano, V. Balzani, *J. Am. Chem. Soc.* **1992**, *114*, 2944; g) P. D. Beer, O. Kocian, R. J. Mortimer, *J. Chem. Soc. Dalton Trans.* **1990**, 3283; h) J. -P. Collin, A. Harriman, V. Heitz, F. Odobel, J. -P. Sauvage, *J. Am. Chem. Soc.* **1994**, *116*, 5679; i) P. D. Beer, Z. Chen, M. G. B. Drew, J. Kingston, M. Ogden, P. Spencer, *J. Chem. Soc. Chem. Commun.* **1993**, 1046; j) B. Delavaux-Nicot, R. Mathieu, D. Montauzon, G. Lavigne, J. -P. Majoral, *Inorg. Chem.* **1994**, *33*, 434.

[9] B. B. Kaul, K. B. Pandeya, *J. Inorg. Nucl. Chem.* **1981**, *43*, 1942.

[10] a) J. A. Cras, J. Willemse in *Comprehensive Coordination Chemistry, The Synthesis, Reactions, Properties & Applications of Coordination Compounds, Vol. 2*, (Ed.: G. Wilkinson, R. D. Gillard, J. A. McCleverty), Pergamon, Oxford, **1987**, pp. 579–593; b) C. Bolzati, L. Uccelli, A. Duatti, M. Venturini, C. Morin, S. Chéradame, F. Refosco, F. Ossola, F. Tisato, *Inorg. Chem.* **1997**, *36*, 3582; c) A. R. Hendrickson, R. L. Martin, N. M. Rohde, *Inorg. Chem.* **1976**, *9*, 2115; d) P. T. Beurskens, J. A. Cras, J. J. Steggerda, *Inorg. Chem.* **1968**, *4*, 810; e) E. A. Pasek, D. K. Straub, *Inorg. Chem.* **1972**, *11*, 259; f) R. Chant, A. R. Hendrickson, R. L. Martin, N. M. Rohde, *Inorg. Chem.* **1975**, *14*, 1894; g) A. R. Hendrickson, R. L. Martin, N. M. Rohde, *Inorg. Chem.* **1974**, *13*, 1933; h) R. Kirmse, S. Saluschke, E. Möller, E. J. Reijerse, E. Gelerinter, N. V. Duffy, *Angew. Chem.* **1994**, *106*, 1546; *Angew. Chem. Int. Ed. Engl.* **1994**, *33*, 1497.

[11] a) A. R. Hendrickson, R. L. Martin, N. M. Rohde, *Inorg. Chem.* **1975**, *14*, 2980; b) J. P. Fackler, Jr., A. Avdeef, R. G. Fischer, Jr., *J. Am. Chem. Soc.* **1973**, *95*, 774; c) A. Avdeef, J. P. Fackler, Jr., R. G. Fischer, Jr., *J. Am. Chem. Soc.* **1970**, *92*, 6972.

[12] A. J. Bard, L. R. Faulkner, *Electrochemical Method*, Wiley, New York, 1980.

[13] M. Ciampolini, L. Fabbrizzi, A. Perotti, B. Seghi, F. Zanobini, *Inorg. Chem.* **1987**, *26*, 3527.

[14] The UV/Vis absorption spectrum of the nickel moiety provides an indication of some concomitant inductive (or solvent) effect which may be mediated through the nickel core: note the appearance of transient absorption near 500 nm in Figure 2 a due to the Ni^{IV} core which increases, reaching a maximum value midway through the oxidation of Ni^{II}, but which eventually disappears at potentials where ferrocenyl subunits are oxidized. The broad band near 500 nm of the Ni^{IV} center reappeared at 0.4 V where the three ferrocenium centers were all reduced.

[15] M. Bonamico, G. Dessy, C. Mariani, A. Vaciago, L. Zambonelli, *Acta. Crystallogr.* **1965**, *19*, 619.

[16] a) J. D. Dunitz, L. E. Orgel, A. Rich, *Acta Cryst.* **1956**, *9*, 373; b) B. L. Shaw, N. I. Tucker, *Organo-Transition Metal Compounds and Related Aspects of Homogeneous Catalysis*, in *Comprehensive Inorganic Chemistry, Chapter 53* (Eds.: J. C. Bailar Jr, H. J. Emeléus, R. Nyholm, A. F. Trotman-Dickenson), Pergamon, Oxford, **1973**, pp. 956–970.

[17] a) C. Levanda, K. Bechgaard, D. O. Cowan, *J. Org. Chem.,* **1976**, *41*, 2700; b) A. -C. Ribou, J. -P. Launay, M. L. Sachtleben, H. Li, C. W. Spangler, *Inorg. Chem.,* **1996**, *35*, 3735; c) S. L. W. McWhinnie, J. A. Thomas, T. A. Hamor, C. J. Jones, J. A. McCleverty, D. Collison, F. E. Mabbs, C. J. Harding, L. J. Yellowlees, M. G. Hutchings, *Inorg. Chem.* **1996**, *35*, 760; d) A. Hradsky, B. Bildstein, N. Schulter, H. Schottenberger, P. Jaitner, K. -H. Ongania, K. Wurst, J. -P. Launay, *Organometallics,* **1997**, *16*, 392; e) R. Rulkens, A. J. Lough, I. Manners, S. R. Lovelace, C. Grant, W. E. Geiger, *J. Am. Chem. Soc.* **1996**, *118*, 12683; f) M. -H. Delville, S. Rittinger, D. Astruc, *J. Chem. Soc. Chem. Commun.* **1992**, 519; g) T. Yoshida, S. Tanaka, T. Adachi, T. Yoshida, K. Onitsuka, K. Sonogashira, *Angew. Chem.* **1995**, *107*, 351; *Angew. Chem. Int. Ed. Engl.* **1995**, *34*, 319; h) C. M. Casado, M. Morán, J. Losada, I. Cuadrado, *Inorg. Chem.* **1995**, *34*, 1668.

[18] a) R. Schneider, A. Riesen, T. A. Kaden, *Helv. Chim. Acta,* **1985**, *68*, 53; b) W. H. Morrison, Jr., S. Krogsrud, D. N. Hendrickson, *Inorg. Chem.* **1973**, *12*, 1998.

[19] a) J. G. Kirkwood, F. H. Westheimer, *J. Chem. Phys.* **1938**, *6*, 506; b) F. H. Westheimer, J. G. Kirkwood, *J. Chem. Phys.* **1938**, *6*, 513; c) P. Paoletti, R. Walser, A. Vacca, G. Schwarzenbach, *Helv. Chim. Acta,* **1970**, *54*, 243; d) L. Fabbrizzi, P. Paoletti, M. C. Zobrist, G. Schwarzenbach, *Helv. Chim. Acta,* **1973**, *56*, 670.

Received: March 25, 1999 [F1697]